Journal of Polymer Research (2022) 29:509
https://doi.org/10.1007/s10965-022-03361-3

ORIGINAL PAPER

Fabrication of nanostructured molecularly imprinted polymer as enantioselective sensor and sorbent for L-phenylalanine benzyl ester

Sajini T[1,2] · Sam John[1] · Beena Mathew[2]

Received: 11 April 2022 / Accepted: 8 November 2022 / Published online: 14 November 2022

Abstract
A novel and unique chiral adsorbent and sensor for an ester of aminoacid, L-phenylalanine benzyl ester (L-PABE), has been synthesised on vinyl group incorporated multiwalled carbon nanotube (MWCNT) using a molecular imprinting approach. In this, molecular imprinted polymers (MIPs) were fabricated by L-PABE as a target molecule supported o MWCNT using methacrylic acid (MAA) as functional monomer and ethylene glycol dimethacrylate (EGDMA) as a crosslinking agent using a simple thermal bulk polymerisation method. Fourier transform infrared spectroscopy (FT-IR), ^{1}H-NMR titration study and UV–Vis. spectroscopic analysis was carried out to investigate the interaction of template-functional monomer complexes formed in the solution earlier to polymerisation. FT-IR, scanning electron microscopy (SEM), X-ray diffraction technique (XRD), thermogravimetric analysis (TGA), and transmission electron microscopy (TEM) were used to determine the structure and morphology of the fabricated polymer-nano composites. The corresponding enantioselective sensor is fabricated on the platinum electrode with imprinted and non-imprinted polymer composites, and their electrochemical parameters were examined by cyclic voltammetry (CV), electrochemical impedance spectroscopy (EIS) and differential pulse voltammetry (DPV). The fabricated MWCNT-MIP established favourable specificity, better sensitivity, maximum stability and a good adsorption capacity for L-PABE molecule compared with the conventional polymer.

Keywords L-PABE · Nano imprinted polymer · Functionalised nanotubes · Electrochemical analysis · Sensor

Introduction

Since chirality and enantiomer recognition possess a significant role and tremendous applications in pharmacology and biology, efficient enantiomer recognition and separation strategies are essential [1, 2]. Many works of literature reveal the importance of enantiomer recognition and separation of chiral compounds in drug designing, separation science and biological systems [3–5]. Various techniques are now available for chiral discrimination, but the selective and specific detection of a single enantiomer is still an interesting analytical task because of the similar physical, chemical, and molecular configurations of enantiomers [6–8]. So it is essential to devise practical, simple, easy and, speedy, accessible techniques for recognising chiral molecules and their separation. In the present article, an ester of amino acid, L-PABE, was selected as the target molecule which prevents sickling of erythrocytes from sickle cell infected patients [9–11].

Here we take advantage of molecular imprinting technology, an emerging method for creating synthetic receptor cavities of the target molecule on a polymer matrix [12, 13]. These fabricated polymers exhibit better selectivity, affinity and specificity toward the target molecule [14, 15]. MIPs possess the remarkable capacity to precisely discriminate one enantiomer and distinguish a single molecule from a mixture of enantiomers [16, 17]. Hence, MIPs were appropriate in many areas of technology like catalysis, biosensors, purification and separation of structurally similar compounds, targeted drug delivery, and biotechnology [18, 19]. The role of MIPs in enantiomer recognition and

✉ Beena Mathew
beenamathew@mgu.ac.in

[1] Department of Chemistry, St. Berchmans College (Autonomous), Mahatma Gandhi University, Changanassery 686101, Kerala, India

[2] School of Chemical Sciences, Mahatma Gandhi University, Priyadarsini Hills P O, Kottayam 686560, Kerala, India

its separation is more significant because the conventional processes are not operative for the current purpose. Because of the easy extraction of template molecules and applicability in a variety of compounds, a non-covalent imprinting strategy is applied throughout the fabrication of MIP [14, 20, 21].

Some problems faced during MIP synthesis are its low selectivity, significant template size limitations and inadequate response kinetic [22–24]. The synthesis of recognition sorbents at nanostructures has significantly improved the elimination of target molecules and hence the binding capacities compared with the classical imprinting techniques [25, 26]. Among various nanoparticles, multiwalled carbon nanotubes (MWCNTs) have received much interest due to their high electrical, thermal and conductivity properties [27–29]. MWCNTs, with exceptionally high surface area, must be effective support material for the fabrication of homogeneous binding sites on a polymer network [30–32]. MIPs wrapped on MWCNTs improve the accessibility of the target molecule and hence diminishes the binding time. To overcome the poor dispersibility character and aggregation properties of MWCNTs, it is necessary to modify MWCNTs via functionalisation [33]. Subsequently, functionalised MWCNTs were treated with appropriate functional monomer, template molecule, initiator, and cross-linker to form the corresponding polymer-nano composites. After the extraction of the target molecule, uniform MIPs were formed on the outer layer of MWCNTs.

In the present article, a novel polymer-nano composite of MIPs with L-PABE as the target molecule was tailored by selective polymerising MIPs onto the vinyl group incorporated MWCNTs. Vinyl-MWCNTs directed selective and specific polymerisation of imprinted polymers by covalent bonds on the exterior part of MWCNTs [22]. For the fabrication of MIPs, compounds bearing functional groups opposite the target molecules are chosen as functional monomers. Here methacrylic acid (MAA) was used as the appropriate functional monomer because of its fundamental nature and ease of availability. MAA should form a pre-polymerised complex with L-phenylalanine benzyl ester via non-covalent interactions comprising electrostatic attraction, hydrogen bonding, and π-π stacking. For the comparative analysis, blank polymers (MWCNT-NIP) were synthesised by the same method without adding the L-PABE molecule during the polymerisation step. To analyse the effect of MWCNTs on chiral recognition and separation, L-PABE imprinted, and non-imprinted polymer (NIPs) without MWCNTs were also synthesised. The corresponding enantioselective sensor is fabricated on a platinum working electrode with both the imprinted and non-imprinted polymers, and their respective electrochemical measurements are determined using cyclic voltammetry (CV), differential pulse voltammetry (DPV) and electrochemical impedance spectroscopy (EIS).

Experimental

Materials and methods

L-PABE and its enantiomer D-PABE (D- phenylalanine benzyl ester) were purchased from Alfa Acer, India. MWCNT of 10–15 nm was obtained from Reinsto Nano ventures private limited, New Delhi, India. The cross-linker, EGDMA, was from Sigma Aldrich, Germany. MAA was from Alfa Acer, India. The initiator, 2,2'-azo-bis-isobutyronitrile (AIBN) and analytical grade methanol solvent are purchased from Merck, India.

Fourier Transform Infrared spectrometer 8400 s (DIN 206–72400), Shimadzu, Japan, was used to record FT-IR spectra of samples. The critical analysis was done on a Shimadzu-UV–vis Spectrophotometer model 2450. The morphological characterisations of the polymer-nano composites were done with transmission electron microscope (TEM) Facility JEOL JEM–2100 and scanning electron microscope (SEM) – JEOL-JSM-6390A. PAN alytical X'PERT PRO was used for the X-ray diffraction analysis of the polymer-nano composites. Thermogravimetric analysis (TGA) was carried out on a NETZSCHSTA449C instrument at room temperature to 500 °C in a nitrogen atmosphere. The whole of the electrochemical measurements, such as cyclic voltammetry (CV), differential pulse voltammetry (DPV), and electrochemical impedance spectroscopy (EIS), were done by a Biologic SP-200 and CHI instrument- CHI08, USA electrochemical workstations.

Characterisation of the pre-polymerised complex of L-PABE and MAA

The basic strategy of MIP fabrication is its conservancy of the host–guest composite structure during the polymerisation process [18]. Hence pre-polymerisation complex formation is essential earlier than polymerisation because the structure of the newly formed composites determines the binding cavity formation, thus affecting the recognition properties of the materials [34, 35]. The higher the stability of the complex, it generates high fidelity binding sites, and MIPs exhibit good recognition ability. Molecular level spectroscopic analyses such as ^{1}H NMR, FT-IR and UV–vis spectroscopic analysis were carried out to investigate the interaction between MAA monomer and the template L-PABE [36]. These spectroscopic techniques also elucidate and rationalise the chiral recognition mechanism during imprinting.

FTIR analysis was done for L-PABE ($0.10 mmol L^{-1}$) solution and a mixture of L-PABE (0.10 mmol/L) and MAA (0.10 mmol/ L) with a resolution of 4 cm^{-1}. For UV–Vis. spectroscopic analysis, a series of test solutions were

prepared with a definite concentration of L-phenylalanine benzyl ester (0.05 mmol/L) and different concentrations of methacrylic acid (0.30–0.90 mmol/L) with pure L-PABE solution in CH_3OH as reference. 1H-NMR investigated the various H-bond interactions between L-PABE and MAA. All spectra were determined at 20 °C with TMS as an internal standard.

Synthesis of polymer-nano composites on vinyl-MWCNTs

MIPs having L-PABE as selective polymerising MIPs fabricated binding cavities onto the vinyl functionalised MWCNT. A 250 ml RB flask with a magnetic stir bar was added 0.02 g MWCNT-CH = CH_2 followed by 30 mL of methanol under a nitrogen atmosphere. In order to form a complex template and functional monomer, L-PABE (0.05 mmol) and MAA (0.10 mmol) dissolved in 5 mL of CH_3OH were added to the RB flask and stirred for 30 min, followed by the addition of initiator AIBN (10 mg) and cross-linker (0.25 mmol) EGDMA. The temperature of the solution was increased to 65 °C, and the reaction was allowed to run for 8 h. The obtained compound was collected by centrifugation and was washed with 70% ethanol to remove the excess reagents. The template molecule was eluted using acetonitrile until there was no absorption peak of L-PABE detected by UV–vis. (at257 nm) in the eluent. The resulting template was washed with ethanol to eliminate the residual acetonitrile and then powdered, dried in vacuum desiccators and filtered to obtain a particle size distribution smaller than 25 µm. The same procedure is used to prepare blank polymers (MWCNT-NIP) to get a better analysis. L-PABE imprinted and non-imprinted polymers without adding MWCNTs were also synthesised and analysed. A schematic representation for the fabrication of MIP and MWCNT-MIP depicted in Scheme 1.

Fabrication of platinum-modified L-PABE sensor and its electrochemical analysis

After polishing the platinum electrode with a 10 µm alumina slurry, it is ultrasonically treated using an ethanol–water mixture for 15 min and then dried. For the modification as a chiral sensor, initially, a mixture of MWCNT-MIP and nafion (0.5%) is prepared and sonicated for 10 min to obtain the composite of MWCNT-MIP/nafion and coated on the polished Pt electrode and then allowed to dry at an average temperature [37, 38]. The modified Pt electrode was designated as Pt/MWCNT-MIP, and the sensor fabrication stages were represented in Scheme 2. The same modification procedure was adopted to prepare Pt/MWCNT-NIP, Pt/MIP and Pt/NIP.

All electrochemical experiments were performed with a three-electrode system comprising a platinum wire (auxiliary electrode), modified Pt electrode (working electrode), and SCE, saturated calomel electrode (reference electrode). For every electrochemical analysis, the modified Pt electrode was immersed into the solution of L-PABE in phosphate buffer solution (PBS) with pH 7.5 for 240 s and then the electrochemical measurements were carried out in a probe solution containing 1:1 $K_3Fe(CN)_6$ [5.0 $mmolL^{-1}$] and KCl [0.1 $molL^{-1}$] and over to the mark with PBS and carried out the measurements at room temperature [39]. The CV scan was carried at a potential range of -0.5 to -1.0 V in the scan rate of 0.01 V s^{-1}. EIS analysis was done in the presence of probe solutions in the frequency range of 100 Hz to 10 kHz at a bias voltage of 0.35 V versus SCE with an amplitude of 5 mV. DPV was determined with a scan rate of 20 V s^{-1}, pulse amplitude 25 mV, pulse width 200 ms, step height 10 mV and step time 500 s.

Affinity, specificity and selectivity analysis of L-PABE imprinted polymer

The amount of L-PABE adsorbed on each polymer-nano composite was analysed using a UV–vis. spectrophotometer at 257 nm. 10 mg of each polymer composite was mixed with 7.0 mL of methanol solution with initial concentrations of L-PABE extending from 0.05 to 0.35$mmolL^{-1}$. The binding process was permitted to continue for 3 h at 28 °C. The obtained mixture was centrifuged at 15000 rpm for 5 min, and the filtrate was examined using a UV–vis. spectrophotometer. The quantity of L-PABE adsorbed Q_e ($\mu molg^{-1}$) onto the polymer-nano composite was calculated per the equation below.

$$Q_e = \frac{(C_i - C_f)V}{m} \tag{1}$$

The binding capacity was measured using the equation [40],

$$Binding\ capacity = \frac{C_i - C_f}{C_i} * 100 \tag{2}$$

where C_f and C_i represent the final and initial concentration of the L-PABE solution.

In the present system, the Langmuir adsorption isotherm model is fit for the adsorption of L-PABE on MWCNT-MIP, which is used for the theoretical evaluation and identification of thermodynamic features [41, 42]. The linear form of Langmuir adsorption isotherm is provided below,

$$\frac{C_e}{Q_e} = \frac{C_e}{Q_m} + \frac{1}{bQ_m} \tag{3}$$

where C_e is the equilibrium concentration, $Q_{e\ is}$ the amount of L-PABE adsorbed at equilibrium, and Q_m is the amount

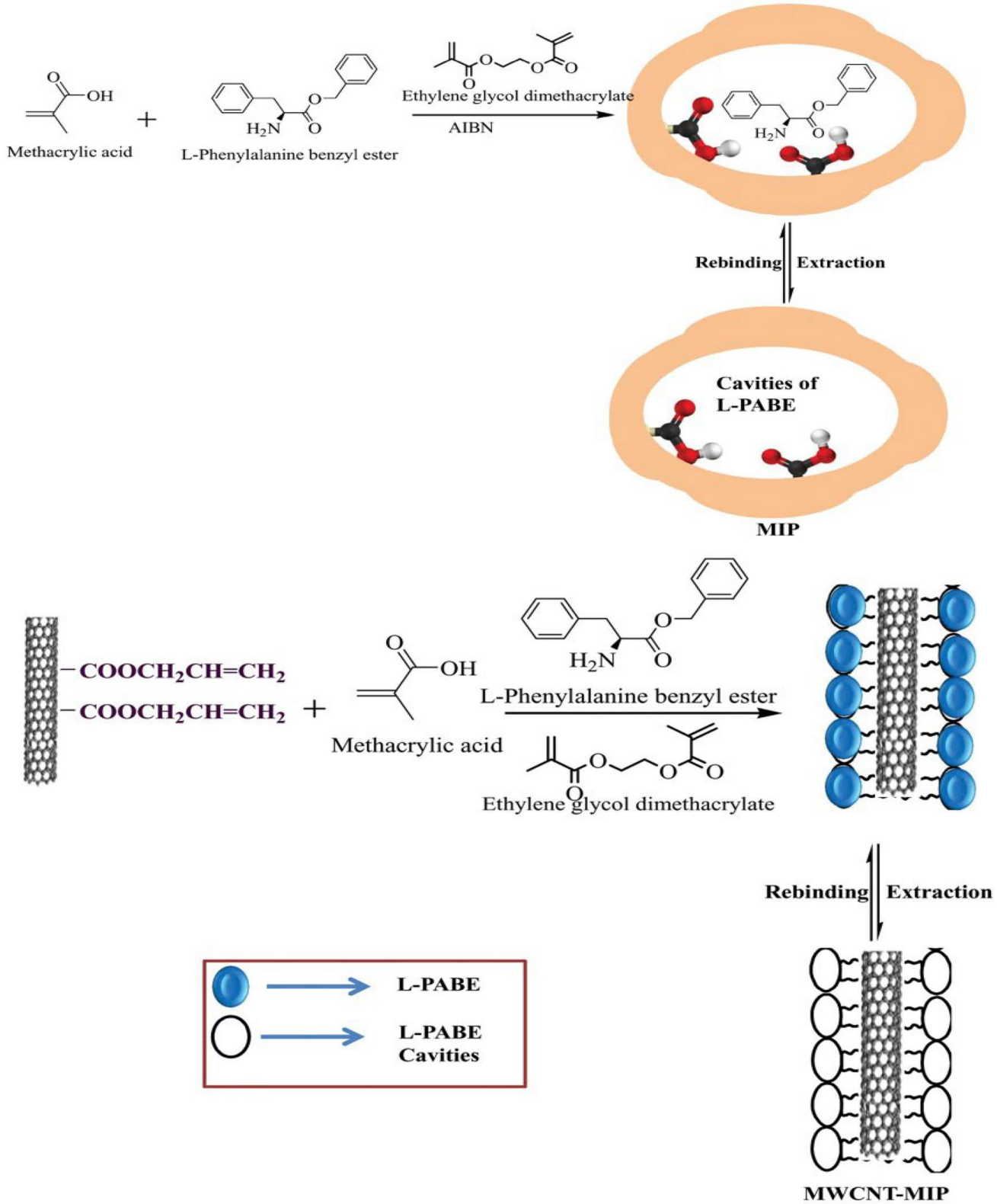

Scheme 1 Schematic representation of synthesis route of MIP and MWCNT-MIP

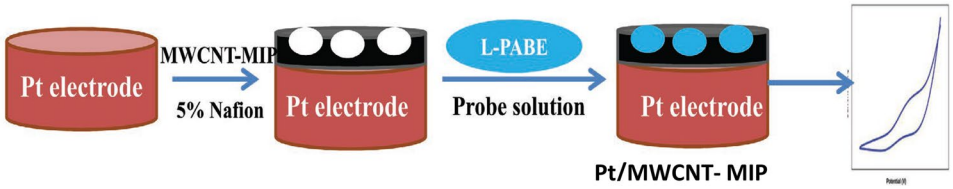

Scheme 2 Schematic representation for the fabrication of Pt/MWCNT-MIP

of L-PABE adsorbed for a complete monolayer. From the graph of specific sorption, C_e/Q_e, against the C_e, the values for Q_m (from the slope) and b (from intercept)are obtained.

For the adsorption dynamics studies, the time taken for the equilibrium rebinding specificity was examined by mixing an equal amount of polymer-nano composites in an L-PABE solution of known concentration. A UV–vis spectrophotometer noticed the quantity of L-PABE adsorbed by MWCNT-MIPs at 257 nm.

For the selectivity studies, to the template desorbed polymer, equal volume of the solutions of template, the enantiomeric analogue, D-PABE and structurally related chiral compounds such as D-phenylalanine and L-phenylalanine having equal concentration were added in different shaking bottles and the difference in the extent of binding was estimated spectrophotometrically. The imprinting factor or separation factor (α), which represents the effect of the imprinting process, is the ratio of the amount of substrate bound by the MIP to that bound by the corresponding NIP.

$$\alpha_{Template} = \frac{K_{MIP}}{K_{NIP}} \tag{4}$$

$$K = \frac{Amount\ of\ bound\ template}{Amount\ of\ free\ template} \tag{5}$$

The selectivity of the imprinted polymer towards the template was calculated in terms of selectivity factor (*a*).

$$a = \frac{\alpha_{Template}}{\alpha_{Analogue}} \tag{6}$$

Results and discussion

Synthesis of polymer-nano composites on vinyl-MWCNTs

Vinyl group incorporated MWCNTs as an excellent support material for the fabrication of MIPs with L-PABE as the target molecule. Vinyl-MWCNT was obtained via a three-stage process: conversion of pure MWCNT into carboxyl functionalised MWCNTs, conversion of MWCNT-COOH to MWCNT-COCl and lastly, the transformation of acylchloride functionalised MWCNT to vinyl-MWCNT. The value of carboxylic acid capacity is found to be 3.05mmolg^{-1}, which revealed the successful transformation of the nanotube into MWCNT-COOH.

Characterisation of the pre-polymerised complex of L-PABE and MAA

FT-IR, 1H-NMR and UV–vis examined the interactions between the L-PABE and MAA. spectrometric measurements. The FT-IR spectrum of 0.10mmolL^{-1} L-PABE solution and that of L-PABE mixed with MAA is given in Fig. 1. In spectrum a, stretching and in-plane bending of > N–H group in L-PABE appeared at 3351 and 1249 cm^{-1}, respectively. Also, > C = O stretching, > C-N stretching and > C-O stretching vibration peaks appeared at 1744, 1019 and 1193 cm^{-1}, respectively. After the mixing of L-PABE and MAA, these characteristics' vibrational peaks changes to 2932 (broad O–H stretching), 1693 (> C = O stretching), 1296 (> C-O stretching), 1021 (> C-N stretching) and 699 (> N–H out of plane bending) cm^{-1} in spectrum c. The formation of a hydrogen bond between L-PABE and MAA decreased the electron cloud density of NH_2 and the vibration frequency.

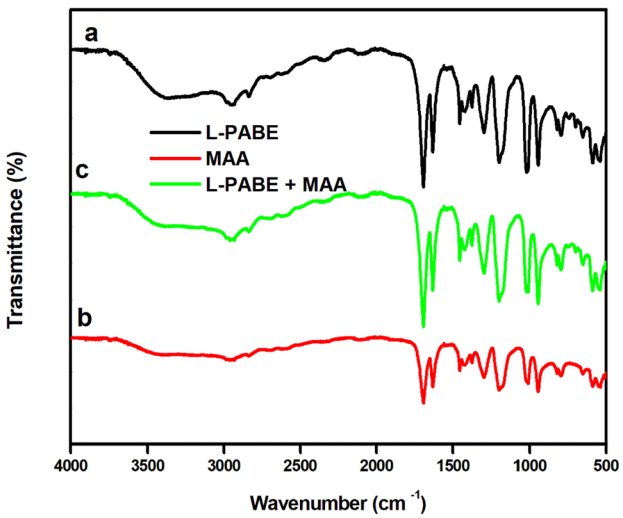

Fig. 1 FT-IR spectra of **a** L-PABE **b** MAA and **c** L-PABE/MAA complex

To examine the stability of the pre-polymerised complexes formed between L-PABE and MAA, UV–vis spectrum analysis was carried out. In this system, the difference spectra of L-PABE (0.05mmolL^{-1}) in methanol is sensitive to the existence of slight amounts of MAA, as shown in Fig. 2.

The results showed that the extreme absorption wavelength of L-PABE shifted remarkably to a longer wavelength, and the maximum absorbance of L-PABE increased with the addition of MAA. The red-shift of the absorption band is characteristic of the hydrogen bonding influence on the π-π* absorption band of a molecule whose chromophore serves as a proton donor [36].

According to the literature [18], for MAA concentration (b_0) more significant than that of L-PABE (a_0), the difference UV absorbance equation of the MAA- L-PABE complex is represented as below:

$$\frac{\Delta A}{b_0^n} = -K\Delta A + K\Delta\varepsilon_c l a_0$$

where ΔA and $\Delta\varepsilon_c$ are the difference absorbency and molar absorptivity of the complex and L-PABE, respectively and K refers to the association constant. The value of K and n are obtained by plotting $\frac{\Delta A}{b_0^n}$ versus ΔA.

In the present system, the plot of $\frac{\Delta A}{b_0^n}$ versus ΔA is a straight line, as shown in Fig. 3. K is measured as 1.1821×10^6 L^2/mol^2 from its slope. It designates that a 1:2 complex dominates in the pre-polymerised complex.

In order to examine the H-bond interaction between L-PABE and MAA, ^{1}H-NMR titration analysis was performed in CD_3OD due to the solubility of L-PABE in methanol. In this system, the amine and carbonyl groups of L-PABE interact with the hydroxyl group of MAA. The addition of MAA to the L-PABE solution resulted in a changing chemical shift of the amine proton of L-PABE towards low-field, as shown in Fig. 4.

If the concentration of MAA is less than that of 0.05 mmolL^{-1}, the chemical shift values are enhanced due to the addition of MAA to the L-PABE solution.

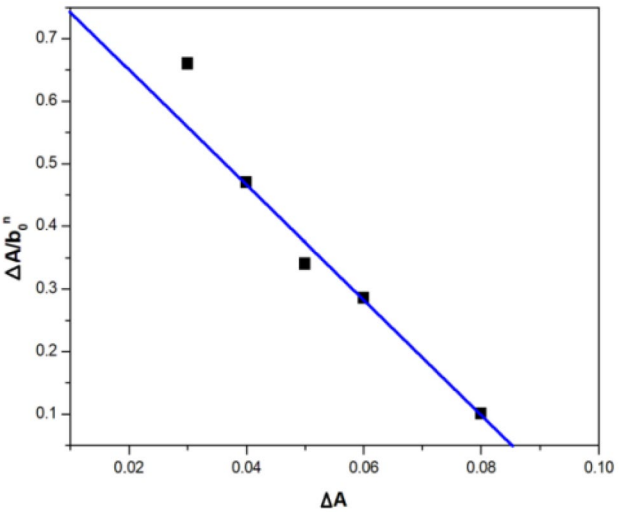

Fig. 3 Plot of $\frac{\Delta A}{b_0^n}$ vs ΔA at 257 nm

Characterisation of MIPs and NIPs

The synthesis of MWCNT-MIP was chiefly characterised by FT-IR spectroscopy evaluation. The FT-IR spectra of vinyl-MWCNT, MIP and MWCNT-MIP are shown in Fig. 5.

The vibrational peaks corresponding to each spectrum of vinyl-MWCNT (a), MWCNT-MIP (b) and MIP(c) are depicted in Table 1.

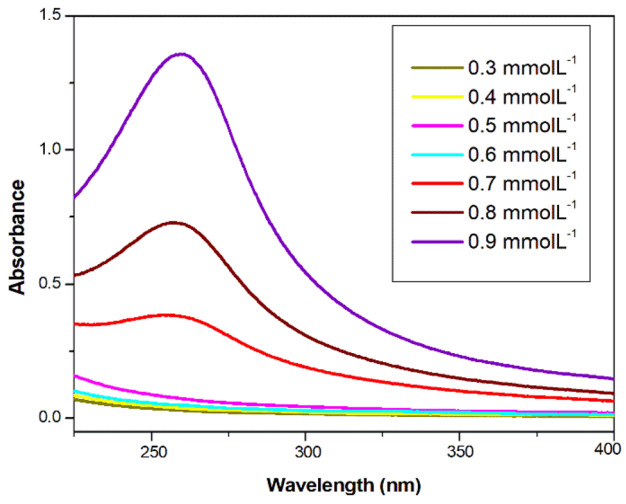

Fig. 2 Difference absorption spectra of L-PABE in the presence of MAA in methanol, a_0 = 0.05mmolL^{-1}, b_0 = 0.30–0.90 mmolL^{-1}

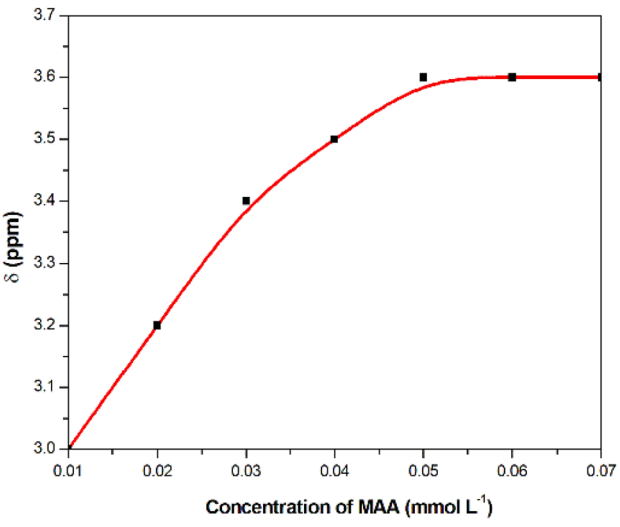

Fig. 4 Chemical shift of amine proton of L-PABE versus the concentration of MAA in the presence of 0.05mmolL^{-1} L-PABE in CD_3OD

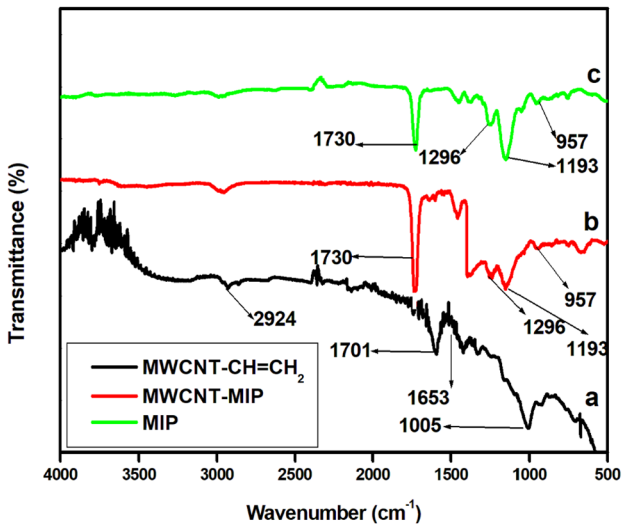

Fig. 5 FT-IR spectra of **a** vinyl-MWCNT, **b** MWCNT-MIP, and **c** MIP

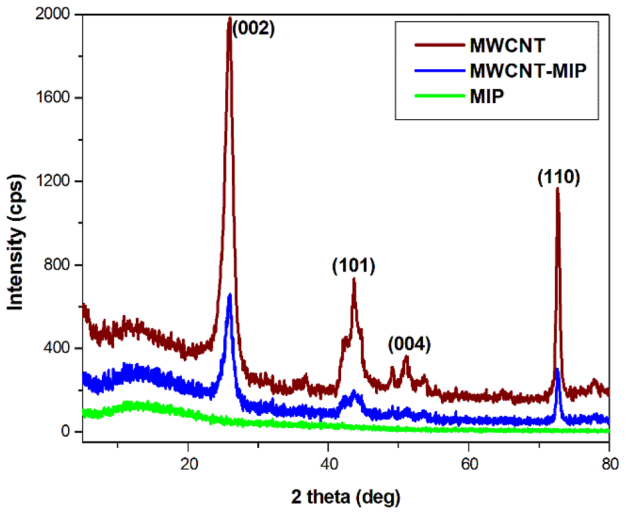

Fig. 6 X-ray diffraction pattern of MWCNT-MIP, MWCNT and MIP

From the table, it is revealed that spectrum (a) consists of all the characteristics of vibrational peaks of vinyl incorporated MWCNT, which indicate the successful fabrication of vinyl-MWCNT. Characteristic vibrational peaks of conventional MIPs were also present in MWCNT-MIP, again indicating the wrapping of the MIP layer on MWCNT-MIP.

Figure 6 depicts the X-ray diffraction patterns of MWCNT, MWCNT-MIP, and conventional MIP. XRD pattern of pure MWCNTs comprises of four characteristic peaks at 25.3°, 43.7°, 51.0° and 72.7° [JCPDS 41–1487] represented the (0 0 2), (1 0 1), (0 0 4), and (1 1 0) planes respectively. The (002) reflection peak was detected at the same 2θ values in both the MWCNT and MWCNT-MIP patterns. The classical MIP contribute an extensive peak range (2θ = 5–20°), proving its amorphous characteristics. From the XRD data, it can be concluded that the MWCNT still had the same cylinder wall. The value of L obtained using Scherrer's formula, $L = 0.9\,\lambda/B\cos\theta$, is found to be 24.5 nm, which is in good agreement with TEM data.

Table 1 FT-IR data of vinyl-MWCNT, MWCNT-MIP and MIP

Sample	Wavenumber (cm^{-1})	Molecular vibrations of functional group
vinyl-MWCNT	2924	> C-H stretching
	1701	> C = O stretching
	1653	> C = C < stretching
	1262	> C-O symmetric stretching (ester
	1005	out of plane > C-H bending vibration
MWCNT-MIP	1730	> C = O stretching
	1021	> C-N stretching
	1296	> C-O symmetric stretching (ester)
	1193	> C-O asymmetric stretching (ester)
	957	> O–H bending
MIP	2952	> C-H stretching
	1730	> C = O stretching
	1021	> C-N stretching
	1296	> C-O symmetric stretching (ester)
	1193	> C-O asymmetric stretching (ester)
	959	> O–H bending

The morphological characteristics of MWCNTs, MWCNT-MIP and MIP were inspected by SEM technique. In Fig. 7, agglomerated nanotube moieties were present in MWCNTs, and MWCNT-MIP showed a nanosized tubular structure with an average size of 22–31 nm. Due to the removal of template molecules from the polymer composites, MIPs had a rough surface and an agglomerated morphology. The agglomerated feature of MIP is converted into nano tubular forms by adding MWCNT in MWCNT-MIP.

To describe the surface characteristics in detail, TEM images were taken for crude MWCNT, vinyl-MWCNT and MWCNT-MIP and depicted in Fig. 8. Because of minute impurities, TEM images of crude MWCNT showed an aggregated, entangled and crosslinked morphology. The agglomeration disappeared in the vinyl functionalised MWCNT, and their average size became 15 nm. Compared with vinyl-MWCNT, the outer layer thickness of MWCNT enhanced MWCNT-MIP and conserved its nanofibrillar structure, and its average size was improved to 25 nm. These parameters indicated that a 5–10 nm thickened MIP layer was effectively covered around the vinyl- MWCNT.

In order to examine the thermal stability of MWCNT, vinyl-MWCNT, MWCNT-MIP and MIP, thermogravimetric analysis was done, and the obtained thermogram is depicted in Fig. 9. The thermogram of purified MWCNT was in the linear form without any degradation up to 500 °C.

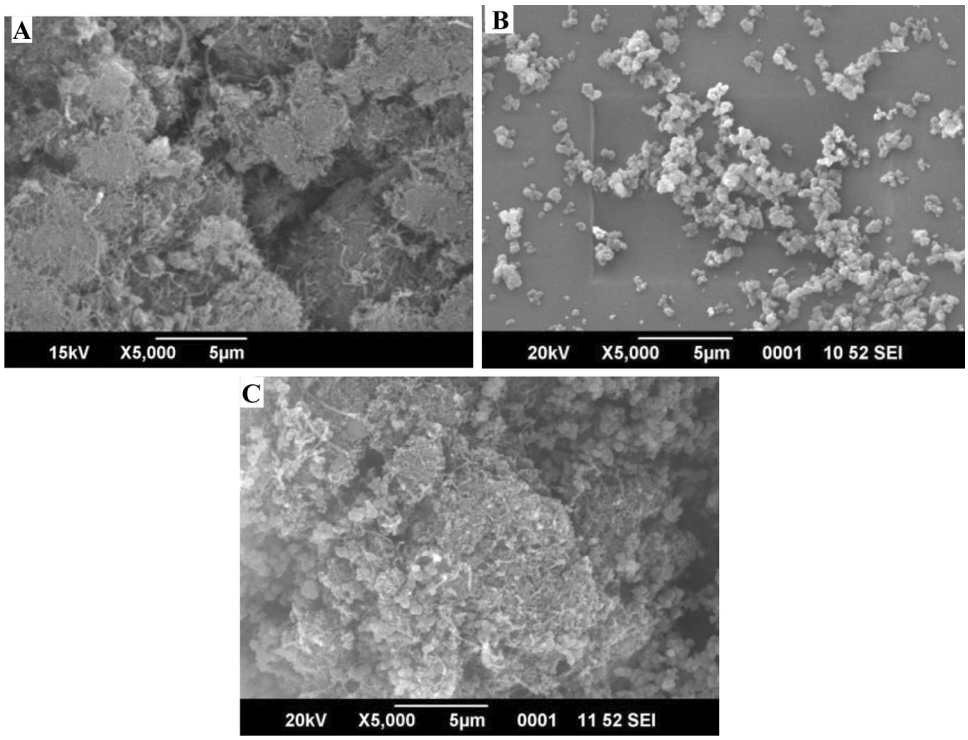

Fig. 7 SEM images of **A** MWCNTs, **B** MIP, and **C** MWCNT-MIP

Vinyl-MWCNT displayed a constant weight loss but not a vast amount (8%) because of the removal of carbonyl groups from MWCNT. The degradation pattern of both the imprinted polymer showed a similar nature. Compared to MWCNT-MIP, bulk MIP showed an enormous weight loss. Bulk MIP began its degradation at 291 °C, though MWCNT-MIP began its decomposition at 297 °C. These thermal parameters indicated better thermal stability possessed by MWCNT-MIP due to the presence of a nano counterpart compared with MIP.

The Raman spectra of purified, vinyl, imprinted, and non-imprinted MWCNT excited with a 514.5 nm laser line are shown in Fig. 10. The most important features seen in purified MWCNT and vinyl functionalized MWCNT are the disorder-induced D band at 1320–1370 cm^{-1}, the tangential G band at 1530–1610 cm^{-1} which is associated with the graphite tangential E_{2g} Raman active mode where the two atoms in graphene unit cell are vibrating tangentially against the other and second order weak bands occur at 2650–2692 cm^{-1}. The radial breathing modes (RBM) observed in the low frequency region 100–200 cm^{-1} is broadened and their intensity is weak. This is related to the large diameter of the MWCNT under investigation. [43].

The BET method analysed the specific surface area analysis of imprinted polymers. Compared to MIP (11.25 m^2g^{-1}), MWCNT-MIP exhibited a higher specific surface area (281.39 m^2g^{-1}). Compared with conventional MIP, nanolayer imprinted polymer possesses a high specific surface area because of the incorporation of MIP on vinyl-MWCNT.

The polarimetric measurement revealed the optical purity of MIPs. MWCNT-MIP displayed an optical purity of 92.8571%, and that of conventional MIP is 79.8642%. The observed specific rotation (α_D^{25}) of L-PABE is -14°.

Voltammetric behaviour of the imprinted and non-imprinted modified electrodes

In order to investigate the electrochemical behaviour of the sensor, Cyclic voltammetry (CV) analysis was carried out [44, 45]. Figure 11 showed the CVs of modified electrodes such as Pt/MWCNT-MIP, Pt/MWCNT-NIP, Pt/MIP and Pt/NIP from -0.5 to -1.0 V at the scan rate of 0.01 V s^{-1} in 10 mM PBS buffer solution (pH 7.5). No measurable redox peak signals were present at the bare Pt electrode because of the absence of a redox probe. An observable redox peak was obtained for Pt/MWCNT-MIP, which revealed that L-PABE possesses an unusual redox reaction as an electroactive redox-probe indicator [46]. The nano counterpart in Pt/MWCNT-MIP offered good electrical conductivity because of their high surface-to-volume ratio and better electrocatalytic activity [47].

NIPs possess a small redox peak current because of the low specificity toward the L-PABE molecule. NIPs do not have any L-PABE recognition sites, its porous sites have some adsorption for the L-PABE molecule and may adsorb the $[Fe\ (CN)6]^{3-}$ or $[Fe(CN)6]^{4-}$ [47].

Electrochemical impedance spectroscopic measurements of Pt/MWCNT-MIP

To examine the probing mechanism of modified electrodes, an ELS analysis was done. The spectra of EIS consist of

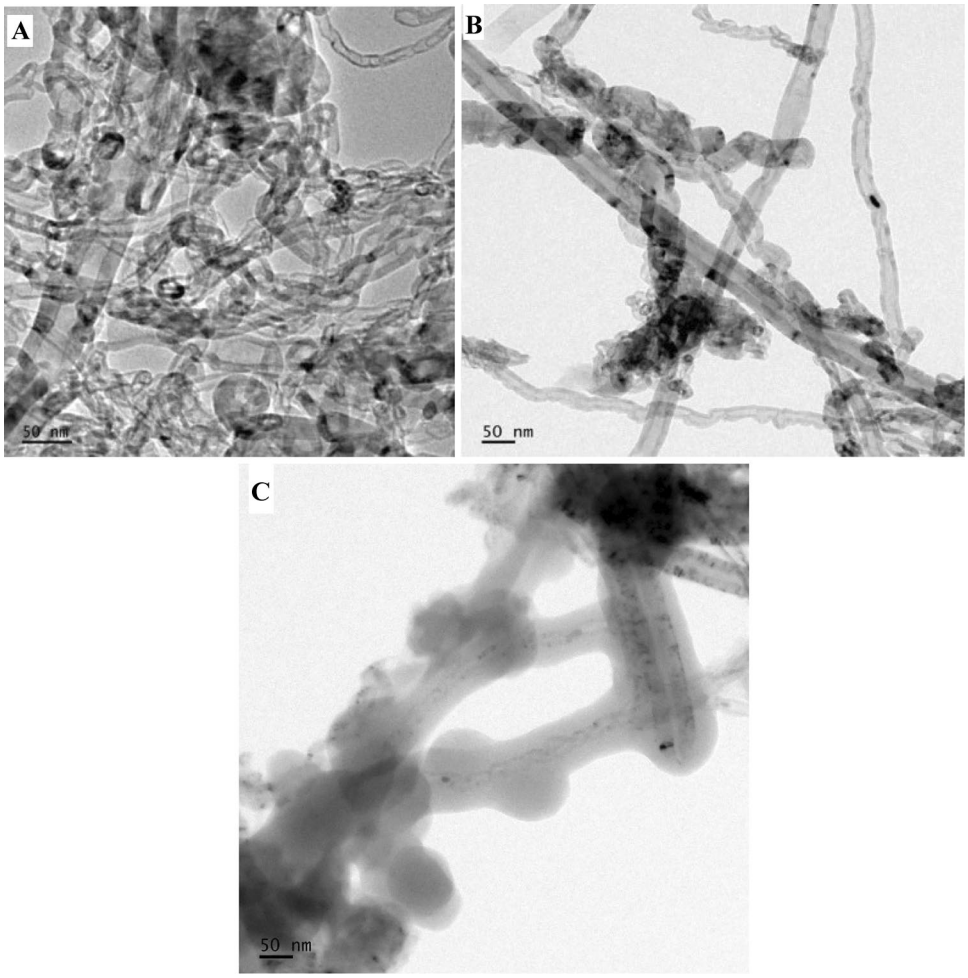

Fig. 8 TEM images of **A** MWCNT, **B** vinyl-MWCNT, and **C** MWCNT-MIP

two major parts, one is a semicircle part at high frequencies, and the other is a linear part in the low-frequency range [39]. The semicircle region and linear part indicated the electron transfer limiting process and diffusion limiting stages of electrochemical reaction [48]. R_{ct}, electron transfer resistance at the surface of the electrode is equivalent to the

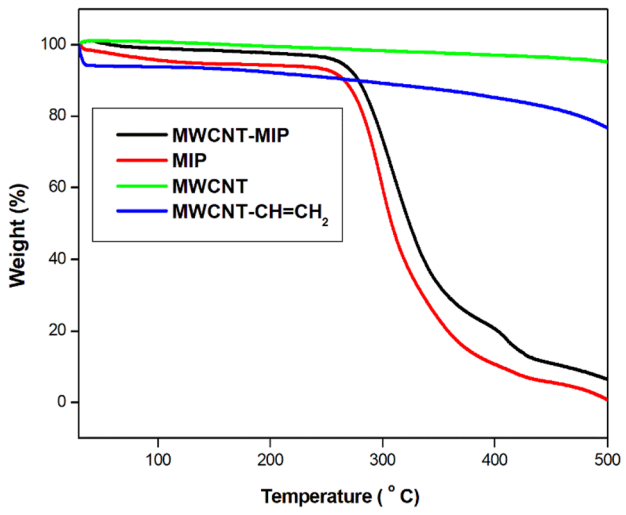

Fig. 9 Thermograms of MWCNT, vinyl-MWCNT, MWCNT-MIP and MIP

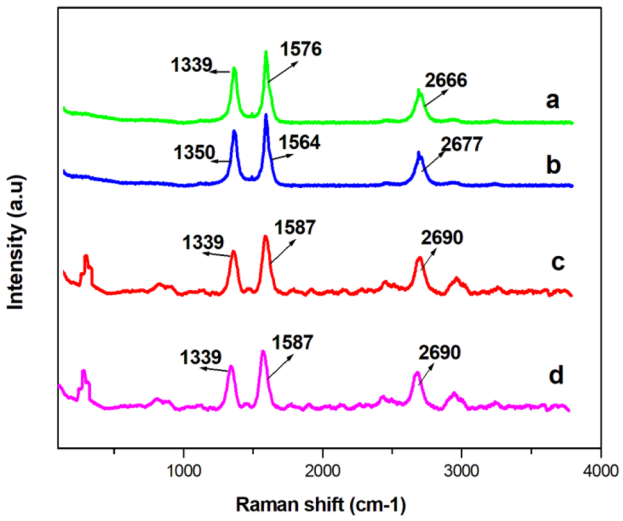

Fig. 10 Raman spectra of **a** MWCNT, **b** vinyl-MWCNT, **c** MWCNT-MIP, and **d** MWCNT-NIP

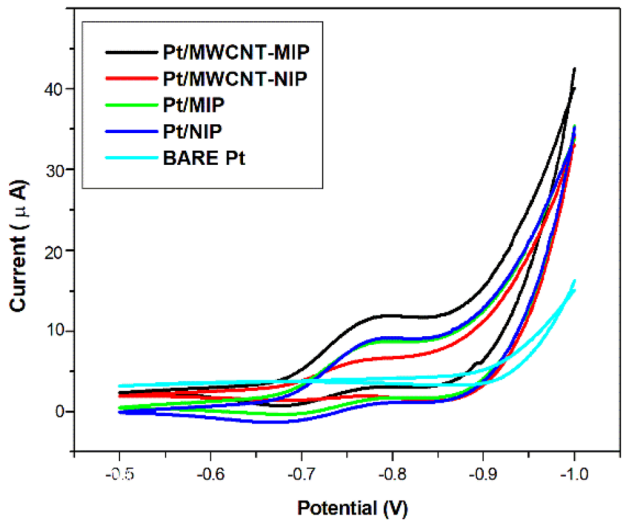

Fig. 11 CVs of bare Pt electrodes and polymer-nano composite modified Pt electrodes. Condition: potential range, -0.5 to -1.0 V; scan rate, 0.01 V s^{-1}; PBS buffer solution (pH 7.5)

diameter of the semicircle region. The obtained EIS data are plotted in Fig. 12.

Figure 12 depicts the Nyquist diagrams of a) bare Pt, b) Pt/MWCNT-MIP, and c) the same electrode Pt/MWCNT-MIP after 240 s incubating in L-PABE (3 µmol L^{-1}) solution. R_{ct} for Pt/ MWCNT-MIP (Fig. 12b) is much lesser than R_{ct} for bare Pt (Fig. 12a). When the surface of the electrode was modified with MWCNT-MIP, R_{ct} was dramatically raised, revealing the very high electron transfer resistance to the redox. In the adsorption process of L-PABE on MWCNT-MIP (Fig. 12c), R_{ct} improved as L-PABE embedded in binding cavities and blocked some arrival channels to the electrode surface. The corresponding impedance parameters are depicted in Table 2.

Optimisation of electrochemical parameters affecting the performance of the sensor

Effect of concentration of L-PABE solution

Figure 13 revealed that the redox peak current increases linearly with the concentration of the L-PABE molecule. This is because of the availability and ease of contact of the electroactive molecules present in the template solution [49]. The saturation of binding cavities at higher template concentrations resulted in a lower peak current. These data again indicated the formation of complementary binding cavities of L-PABE molecules on polymer-nano composites. The fabricated complementary sites with similar size and conformation are available for better adsorption during the process [48].

Impact of pH

The electrochemical performance of the modified sensor is mainly affected by the pH of the solution. Influence of pH of phosphate buffer solution (PBS) was investigated over the pH range 6.5 to 8.5 and depicted in Fig. 14. It was found that the maximum current response was obtained at a pH of 7.5 whereas all the other pH values didn't show

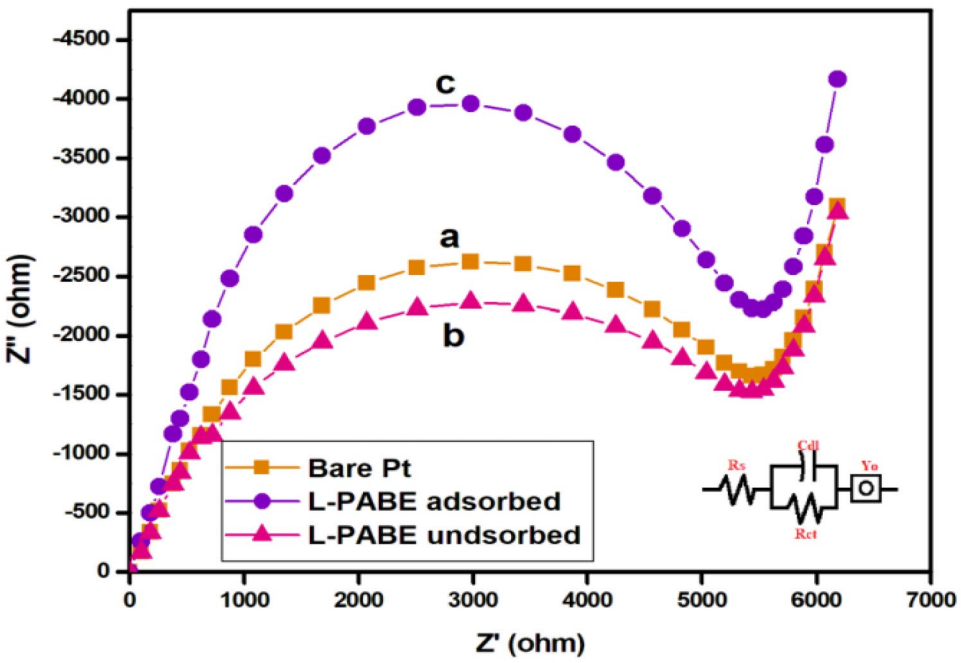

Fig. 12 Electrochemical impedance spectra of $K_3Fe(CN)_6$ and KCl at **a** bare Pt, **b** Pt/MWCNT-MIP and **c** the same electrode, Pt/MWCNT-MIP after 240 s incubating in L-PABE solution. Inset represents the corresponding equivalent circuit of EIS

Table 2 Impedance parameters of bare Pt electrode, L-PABE desorbed, and L-PABE adsorbed electrodes

Impedance parameters	Platinum electrode		
	Bare (a)	L-PABE desorbed (b)	L-PABE adsorbed (c)
Solution resistance, R_s (Ω)	155.1	117.5	234.8
Capacitance, C_{dl} (F)	1.29×10^{-8}	1.519×10^{-8}	7.729×10^{-9}
Charge transfer resistance, R_{ct} (Ω)	4233	3556	6564
Admittance, Y_o (S)	1.203×10^{-5}	1.225×10^{-5}	9.123×10^{-6}

any electrochemical current response. Hence pH 7.5 was selected for electrochemical detection of L-PABE.

Influence of the template on the functional monomer mole ratio

To get a better recognition of binding sites of MIP layered on MWCNT with the template, varying ratios of functional monomer (MAA) and L-PABE were investigated on the response of Pt/MWCNT-MIP in probe solution. For this purpose, the electrochemical response of the modified electrode was examined by changing monomer-to-template ratio as 1:1, 1:2, 1:3, 1:4, and 1:5 and the determined data were plotted in Fig. 15. When the ratio was increased, the current response increased steeply which ascribed to the fact that the rise in the amount of functional monomer imparted more approachable cavities in the MIP layer. Consequently, ferricyanide could reach to the surface of the electrode resulting in an enhancement in peak current. Further increase of monomer concentration diminishes the peak current caused the MIP layer to grow thick, and many binding sites were buried in the polymeric network and turned into ineffective binding sites for L-PABE sorption [48]. In the ratio of 1:2 MAA to L-PABE, optimum numbers of MIP cavities were covered by the template molecule. Hence the largest current response of probe solution to the modified electrode was obtained in 1:2 ratio.

Influence of scan rate

To investigate the electrochemical mechanism, peak current versus scan rate analysis is depicted in Fig. 16. Figure 16a, b reveal a better linear relationship between peak current and scan rate and a good correlation coefficient between anodic or cathodic peak current and scan rate, respectively. All these results suggested that the electrochemical mechanism is similar to a surface-controlled quasi-reversible process [50].

Evaluation of the effect of incubation time

The impact of incubation time on the peak current was investigated by CV analysis to find out the optimum time for maximum L-PABE adsorption on the fabricated electrochemical sensor. After the extraction of L-PABE from the MWCNT-MIP layer, the Pt electrode was incubated in 1.0 μmolL^{-1} template solution at pH = 7.5 at different times, and then the electrode was immersed into the probe solution to determine the current signal. Figure 17 narrates the redox peak current response concerning incubation time. Initially, more binding cavities were available,

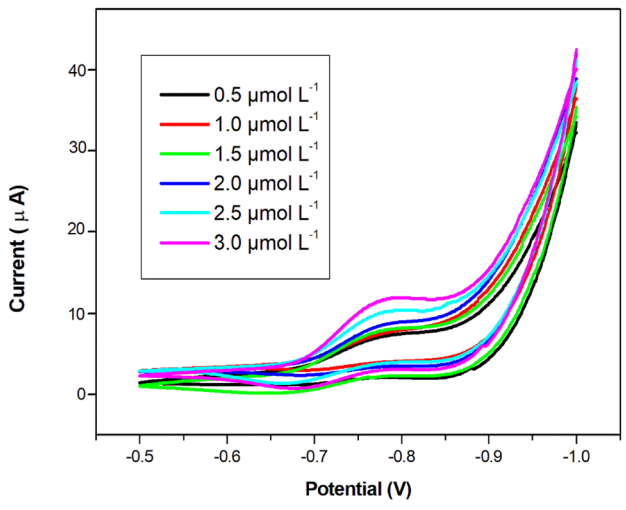

Fig. 13 CVs of Pt/MWCNT-MIP in the presence of L-PABE solution at varying concentrations

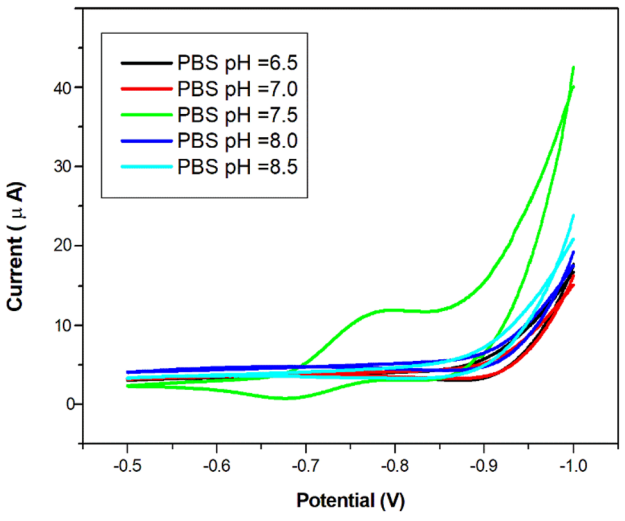

Fig. 14 CVs of Pt/MWCNT-MIP in the presence of L-PABE solution at varying pH

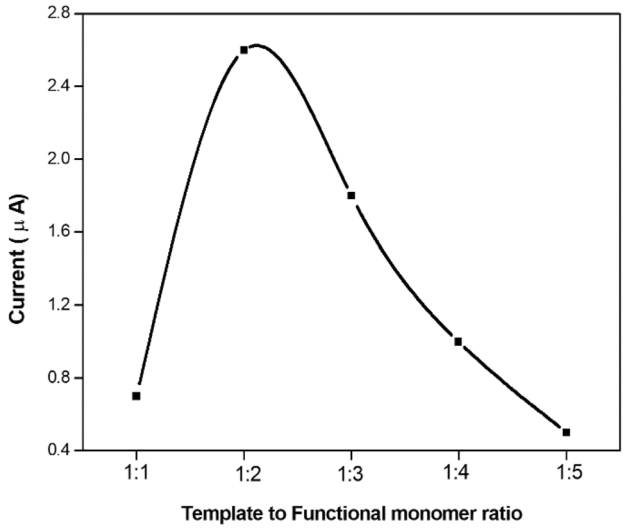

Fig. 15 Redox peak current response of Pt/MWCNT-MIP electrode with varying L-PABE/MAA

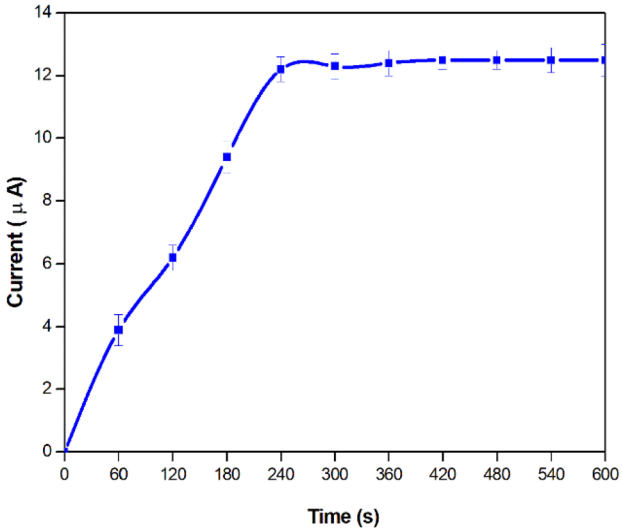

Fig. 17 Plot of current versus incubation time

hence a significant peak current signal up to 4 min. Most of the binding cavities were filled with L-PABE molecules, which then turned into the state of saturated condition at a higher incubation time. Hence 4 min was chosen as the optimum incubation time for further electrochemical studies.

Selectivity analysis of the modified sensor towards the template molecule

To determine the selectivity of the Pt/MWCNT-MIP, the peak current response of the sensor towards L-PABE (3 μmol L^{-1}) and its enantiomer D-PABE (3 μmol L^{-1}) were determined, and the corresponding CVs are plotted in Fig. 18. The redox peak current of Pt/MWCNT-MIP towards L-PABE was more significant than that of D-PABE. This is because of the fabrication of complementary chiral recognition sites of L-PABE on the polymer matrix. The fabricated sites were unavailable to bind its enantiomer D-PABE tightly, therefore, obtaining the lower peak current. The modified electrode exhibited higher selectivity and specificity towards the L-PABE than the D-PABE molecule.

Determination of LOD and LOQ of the modified sensor

DPV technique was used to evaluate the limit of detection (LOD) and limit of quantification (LOQ) of the modified

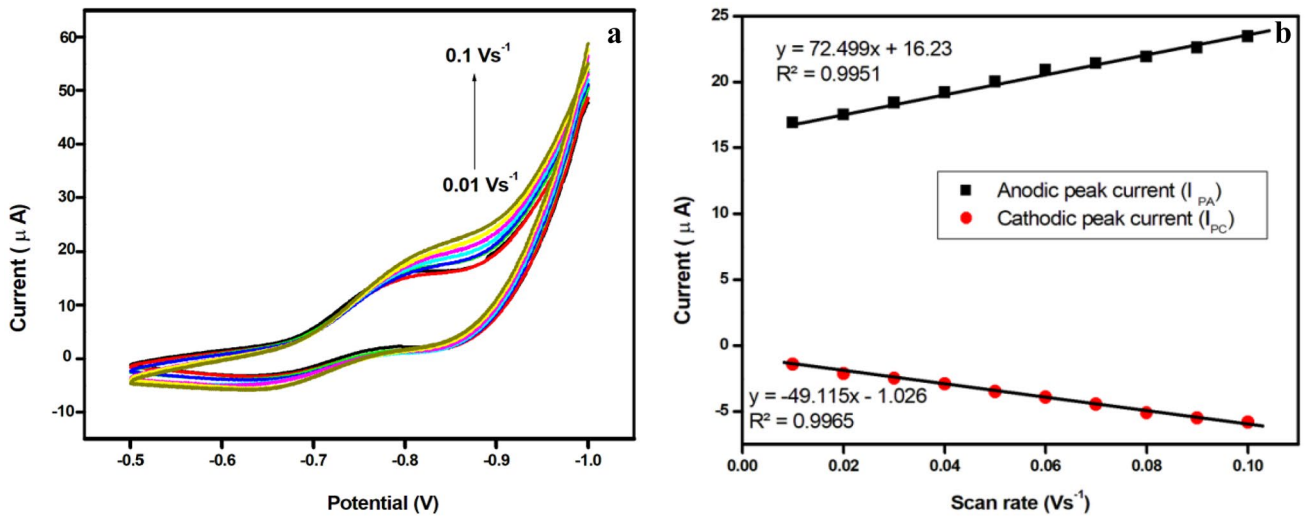

Fig. 16 **a** CVs of Pt/MWCNT-MIP containing L-PABE molecule at different scan rates (10 to 100 mVs^{-1}) and **b** relationship between anodic and cathodic peak current with a scan rate

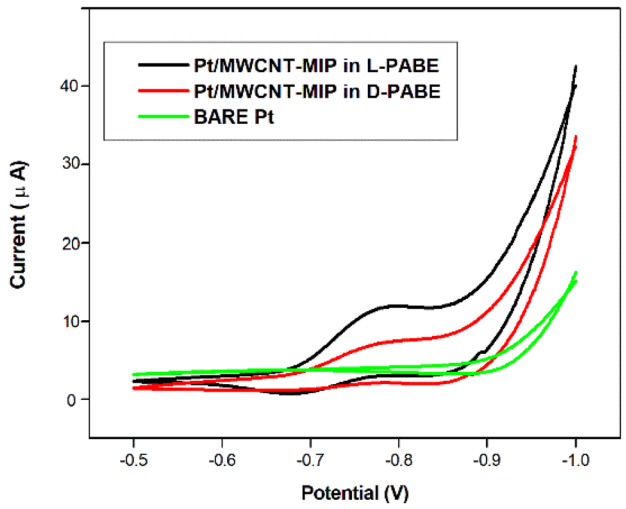

Fig. 18 Selectivity of the Pt /MWCNT-MIP towards L-PABE and D-PABE

sensor for L-PABE under optimised conditions [51, 52]. Under optimised conditions, DPV measurement was done and plotted in Fig. 19. As the concentration increases, the peak current also increases. The DPV curve found the LOD and LOQ to be 0.3388 μmol L^{-1} and 1.1295 μmol L^{-1}, respectively.

Adsorption analysis of MIPs and NIPs

An equilibrium binding analysis was done to find the imprinted polymer- nanocomposites- binding performance against the control non-imprinted polymer. The obtained data is depicted in Fig. 20, indicating that a finite number of binding cavities are formed in the imprinted polymer during the imprinting process. Also, due to the incorporation of a nano counterpart, the adsorption capacity of MWCNT-MIP was greater than that of bulk MIP. Because of the complementary cavity formation, MWCNT-MIP exhibited a higher binding capacity than non-imprinted MWCNT-NIP. In MWCNT-NIP, non-specific interaction happened and hence weak adsorption towards L-PABE.

In Langmuir isotherm, the plots of specific sorption, C_e/Q_e, against the equilibrium concentration, C_e, for MWCNT-MIP polymer and MIP were plotted, as depicted in Fig. 21. The correlation coefficient (r) of MWCNT-MIP is determined as 0.9988, indicating that the adsorption process was mainly monolayer on a homogeneous adsorbent surface. The Langmuir constants of MWCNT-MIP, Q_m and b, were 150.04 μmolg^{-1} and 0.0366 Lmmol^{-1}, respectively.

Figure 22 shows the time dependence of the adsorption capacities of L-PABE towards imprinted and non-imprinted polymer as a function of time. As shown, L-PABE adsorption initially increased and then increased slowly with the time extension. The adsorption process became saturated at 40 min in MWCNT-MIP. A large number of binding cavities are available initially and become saturated finally.

The sorption kinetics data of L-PABE were analysed using the Langergen pseudo-second-order equation based on adsorption equilibrium capacity may be expressed in the form:

$$\frac{t}{Q_t} = \frac{1}{k_2 Q_e^{\,2} + \frac{t}{Q_e}}$$

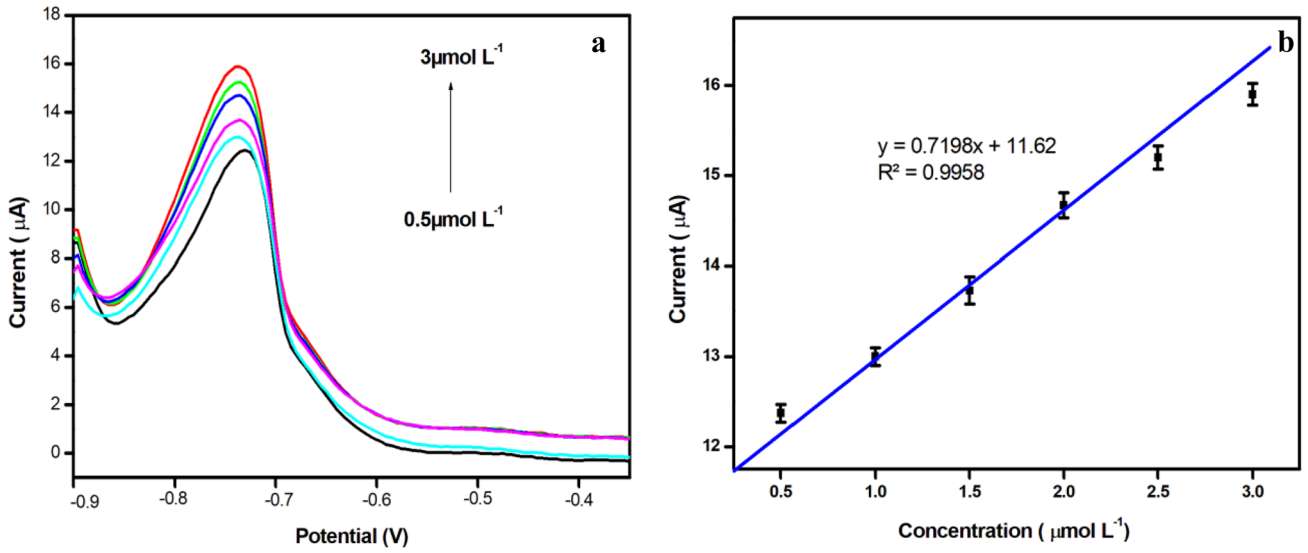

Fig. 19 **a** Cyclic voltammogram for Pt/MWCNT-MIP containing L-PABE molecule at various scan rates ranging from 10 to 100 mVs^{-1} and **b** linear relationship of anodic and cathodic peak current versus scan rate

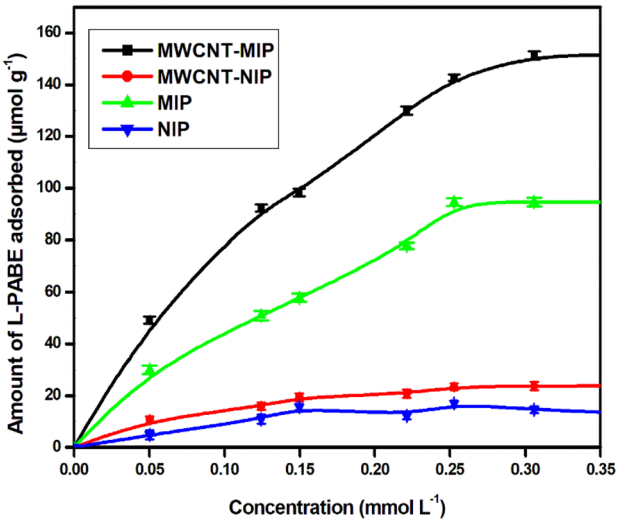

Fig. 20 Binding isotherm of MWCNT-MIP, MWCNT-NIP, MIP, and NIP

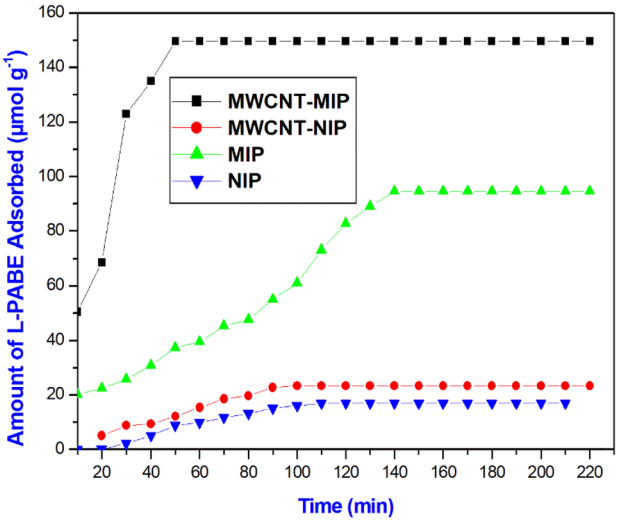

Fig. 22 The adsorption kinetics on imprinted and non-imprinted polymer

where k_2 is the rate constant of pseudo-second-order sorption.

The plot of t/Q_e against t, which is given in Fig. 23, has a high correlation coefficient (0.9992), indicating that the L-PABE adsorption using MWCNT-MIP obeys the second order kinetics reaction with rate constant $k_2 = 0.2413$ mol^{-1} min^{-1}.

The chiral recognition capacity of synthesised MWCNT-MIP was evaluated using its chiral analogue D-LABE and depicted in Fig. 24. The non-imprinted polymer prepared without adding the template molecule could not recognise the chirality. Due to the formation of non-specific binding cavities in the polymer network, non-imprinted composites cannot recognise L-PABE. The Qe value of MWCNT-MIP towards L-PABE and D-LABE is 149.7 and 25.8 μmolg^{-1}, respectively. This result revealed that the interaction between the MAA and L-PABE should be crucial in fabricating the adsorption cavities. The shape or sites constructed on the polymer surface were complementary to the imprinted L-PABE and should have a vital role in recognising the molecular chirality.

Table 3 showed that MWCNT-MIP possessed high selectivity than conventional MIP. This indicated that the nano counterpart helps form the homogenous binding sites in MWCNT-MIP. Consequently, a higher number of template recognition sorbents was formed in the surface of MWCNT-MIP and exhibited high affinity towards the L-PABE molecule. The high specificity is mainly attributed to the unique binding of the imprinted sites to the template molecule, so they cannot bind the other analogues tightly.

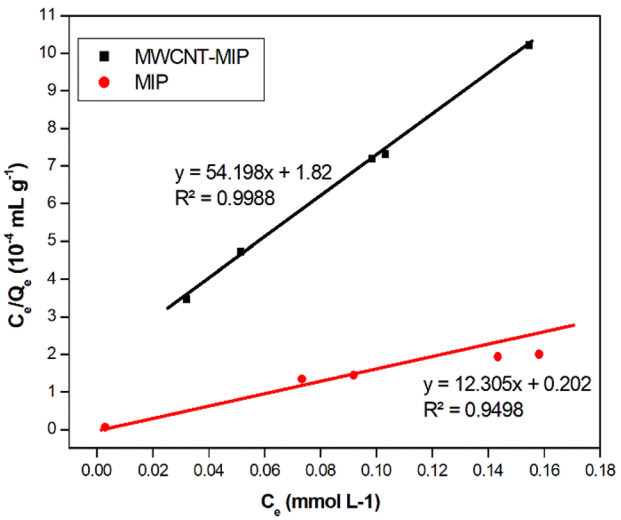

Fig. 21 Langmuir isotherms of MWCNT-MIP and MIP

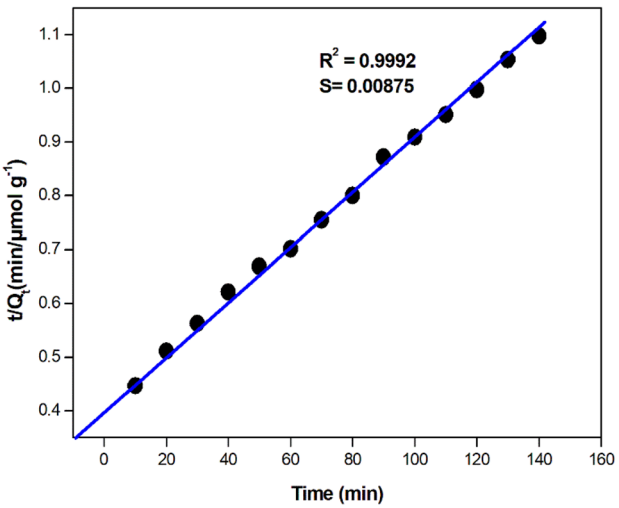

Fig. 23 Second order kinetics curve of MWCNT-MIP

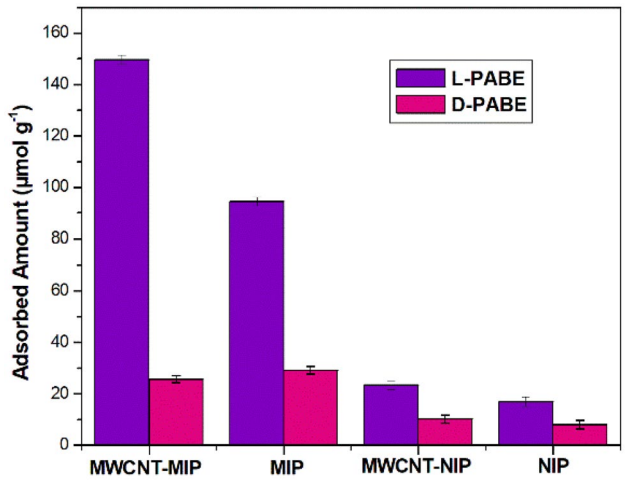

Fig. 24 Selectivity analysis of the L-PABE imprinted and non-imprinted polymers

Table 3 Selectivity factor of the polymer

	Separation factor of L-PABE	Separation factor of D-PABE	Selectivity factor
MWCNT-MIP	14.2345	2.7032	5.2658
MIP	8.2949	3.2717	2.5353

Conclusions

A novel chiral sorbent and sensor for enantioselective recognition for L-PABE are successfully tailored on vinyl-MWCNT via molecular imprinting technique. The complementary nature of the template and functional monomer were obtained in the pre-polymerised complex studies. The complex formed between MAA and L-PABE is preserved within a matrix to form a chemically and sterically complementary imprint to the template. The fabricated MWCNT-MIP showed favourable selectivity, good stability and a higher adsorption capacity for the template molecule than conventional MIP. Electrochemical measurements revealed that the platinum-modified electrode with MWCNTs as supporting material is a promising sensor for analysing the L-PABE chiral compound. The LOD and LOQ values of the Pt/MWCNT-MIP were 0.3388 µmol L^{-1} and 1.1295 µmol L^{-1}, respectively. The results of the high adsorption amount of MWCNT-MIP particles for L-PABE adsorption suggest that the nanolayer MIP preparation on the surface of the MWCNTs could enhance the porous site availability compared to conventional polymerisation. FT-IR spectroscopy, TEM, SEM and XRD confirmed the homogeneous formation of MWCNT-MIP binding sites. The Langmuir adsorption isotherm again confirmed the homogeneity. The adsorption kinetics of L-PABE on MWCNT-MIP agreed with the second-order rate equation.

Acknowledgements First author, T. Sajini, acknowledge all the support provided by University Grants Commission, India through the Faculty Development Programme.

Data availability statement Data are available upon reasonable request.

Declarations

Conflict of interest There are no conflicts to declare.

References

1. Dzgoev A, Haupt K (1999) Enantioselective molecularly imprinted polymer membranes. Chirality. 469:465–469
2. Chang C, Wang X, Bai Y, Liu H (2012) Applications of nanomaterials in enantioseparation and related techniques. Trends Anal Chem 39:195–206. https://doi.org/10.1016/j.trac.2012.07.002
3. Ramström O, Gustavsson PE, Ye L (1998) Chiral recognition by molecularly imprinted polymers in aqueous media. Chromatographia 48:197–202
4. Trojanowicz M, Kaniewska M (2009) Electrochemical chiral sensors and biosensors. Electroanalysis 3:229–238. https://doi.org/10.1002/elan.200804382
5. Ou J, Dong J, Tian T, Hu J, Ye M, Zou H (2007) Enantioseparation of tetrahydropalmatine and Tröger ' s base by molecularly imprinted monolith in capillary electrochromatography. J Biochem Biophys Methods 70:71–76. https://doi.org/10.1016/j.jbbm.2006.07.003
6. Ingole PG, Bajaj HC, Singh K (2016) Enantiomeric separation of α-amino acids by imprinted terpolymer membrane. Arab J Chem 9:960–965. https://doi.org/10.1016/j.arabjc.2011.10.011
7. Wang JF, Zhou LM, Liu XL, Wang QH, Zhu DQ (2000) Simultaneous chiral separation using a combinatorial molecular imprinting phase. Chinese Chem Lett 11:65–68
8. Maier NM, Lindner W (2007) Chiral recognition applications of molecularly imprinted polymers : a critical review. Anal Bioanal Chem 389:377–397. https://doi.org/10.1007/s00216-007-1427-4
9. Sajini T, Thomas R, Mathew B (2019) Computational design and fabrication of enantioselective recognition sorbents for l-phenylalanine benzyl ester on multiwalled carbon nanotubes using molecular imprinting technology. Chin J Polym Sci 37:1305–1318. https://doi.org/10.1007/s10118-019-2282-4
10. Acquaye CTA, Gorecki M, Wilchek M, Votano JR, Rich A (1980) Antisickling activity of amino acid benzyl esters. Proc Natl Acad Sci USA 77:181–185
11. Acquaye CTA, Young JD, Ellory JC, Gorecki M, Wilchek M (1982) Mode of transport and possible mechanism of action of L-phenylalnine benzyl ester as an anti-sickling agent. Biochim Biophys Acta 693:407–416
12. Zhong C, Yang B, Jiang X, Li J (2018) Current progress of nanomaterials in molecularly imprinted electrochemical sensing. Crit Rev Anal Chem 48:15–32. https://doi.org/10.1080/10408347.2017.1360762
13. Chemie O, Bonn BDU, Sarhan A (1977) Enzyme-analogue built polymers; On the synthesis of polymers containing chiral cavities and their use for the resolution of racemates. Makromol Chem 178:2799–2816
14. Lingxin S, Wang X, Lu W, Wu X, Li J (2016) Molecular imprinting : perspectives and applications. Chem Soc Rev 45:2137–2211. https://doi.org/10.1039/C6CS00061D

15. Komiyama M, Mukawa T (2003) Molecular imprinting from fundamentals to applications. Wiley-VCH, Weinheim
16. Ertürk G, Mattiasson B (2017) Molecular imprinting techniques used for the preparation of biosensors. Sensors 17:288–305. https://doi.org/10.3390/s17020288
17. Hosoya K, Shirasu Y, Kimata K, Tanaka N (1998) Molecularly imprinted chiral stationary phase prepared with racemic template. Anal Chem 70:943–945
18. Lu Y, Li C, Zhang H, Liu X (2003) Study on the mechanism of chiral recognition with molecularly imprinted polymers. Anal Chim Acta 489:33–43. https://doi.org/10.1016/S0003-2670(03)00708-6
19. Yoshida M, Hatate Y, Uezu K, Goto M (2000) Chiral-recognition polymer prepared by surface molecular imprinting technique. Colloids Surf A Physicochem Eng Asp 169:259–269
20. Sajini T, Gigimol MG, Mathew B (2019) Kinetic and thermodynamic studies of molecularly imprinted polymers for the selective adsorption and specific enantiomeric recognition of D -mandelic acid. J Polym Res 26:88. https://doi.org/10.1007/s10965-019-1746-0
21. Spivak DA (2005) Optimisation, evaluation, and characterisation of molecularly imprinted polymers. Adv Drug Deliv Rev 57:1779–1794. https://doi.org/10.1016/j.addr.2005.07.012
22. Kan X, Zhao Y, Geng Z, Wang Z, Zhu J (2008) Composites of multiwalled carbon nanotubes and molecularly imprinted polymers for dopamine recognition. J Phys Chem C 112:4849–4854
23. Xu L, Xu Z (2012) Molecularly imprinted polymer based on multiwalled carbon nanotubes for ribavirin recognition. J Polym Res 19:1–6. https://doi.org/10.1007/s10965-012-9942-1
24. Rezaei B, Rahmanian O (2012) Direct nanolayer preparation of molecularly imprinted polymers immobilised on multiwalled carbon nanotubes as a surface-recognition sites and their characterisation. J Appl Polym Sci 125:798–803. https://doi.org/10.1002/app.35383
25. Balasubramanian K, Burghard M (2005) Chemically functionalised carbon nanotubes. Small 1:180–192. https://doi.org/10.1002/smll.200400118
26. Scida K, Stege PW, Haby G, Messina GA, Garcia CD (2012) Recent applications of carbon-based nanomaterials in analytical chemistry. Anal Chim Acta 691:6–17. https://doi.org/10.1016/j.aca.2011.02.025
27. Hone J (2004) Carbon nanotubes : thermal properties. Dekker Encyclopedia of Nanoscience and Nanotechnology, Marcel Dekker, Newyork. https://doi.org/10.1081/e-enn10.1081/e-enn120009128
28. Ciraci S, Dag S, Yildirim T, Gulseren O, Senger RT (2004) Functionalised carbon nanotubes and device applications. J Phys Condens Matter 16:901–960. https://doi.org/10.1088/0953-8984/16/29/r01
29. Valle M, Pumera M, Llopis X, Pe B (2005) New materials for electrochemical sensing VI : carbon nanotubes. Trends Anal Chem 24:826–838. https://doi.org/10.1016/j.trac.2005.03.019
30. Belin T, Epron F (2005) Characterisation methods of carbon nanotubes : a review. Mater Sci Eng B 119:105–118. https://doi.org/10.1016/j.mseb.2005.02.046
31. Seetharamappa J, Yellappa S, D'Souza F (2006) Carbon Nanotubes : next generation of electronic materials. Electrochem Soc Interface 15:23–26
32. Yang W, Thordarson P, Gooding JJ, Ringer SP, Braet F (2007) Carbon nanotubes for biological and biomedical applications. Nanotechnology 18:412001. https://doi.org/10.1088/0957-4484/18/41/412001
33. Rosca ID, Watari F, Uo M, Akasaka T (2005) Oxidation of multiwalled carbon nanotubes by nitric acid. Carbon N Y 43:3124–3131. https://doi.org/10.1016/j.carbon.2005.06.019
34. Zhang H, Song T, Zong F, Chen T, Pan C (2008) Synthesis and characterisation of molecularly imprinted polymers for phenoxyacetic acids. Int J Mol Sci 9:98–106
35. Mahony JO, Karlsson BCG, Nicholls IA (2007) Correlated theoretical, spectroscopic and X-ray crystallographic studies of a non-covalent molecularly imprinted polymerisation system. Analyst 132:1161–1168. https://doi.org/10.1039/b706258c
36. Shen Z, Zhu X, Yang J, Cai J, Su Q (2008) Study on the binding characteristic of methamidophos-specific molecularly imprinted polymer and the interactions between template and monomers. J Chinese Chem Soc 55:587–593
37. Aravind A, Mathew B (2018) Tailoring of nanostructured material as an electrochemical sensor and sorbent for toxic Cd (II) ions from various real samples. J Anal Sci Technol. https://doi.org/10.1186/s40543-018-0153-1
38. Elugoke SE, Adekunle AS, Fayemi OE, Akpan ED, Mamba BB, Sherif E-SM, Ebenso EE (2021) Molecularly imprinted polymers (MIPs) based electrochemical sensors for the determination of catecholamine neurotransmitters – Review. Electrochem Sci Adv 1:e2000026. https://doi.org/10.1002/ELSA.202000026
39. Rezaei B, Rahmanian O, Ensafi AA (2014) An electrochemical sensor based on multiwall carbon nanotubes and molecular imprinting strategy for warfarin recognition and determination. Sens Actuators B Chem 196:539–545. https://doi.org/10.1016/j.snb.2014.02.037
40. Yusof NA, Beyan A, Harson MJ, Ibrahim NA (2010) synthesis and characterisation of a molecularly imprinted polymer for Pb2+ uptake using 2-vinylpyridine as the complexing monomer. Sains Malaysiana 39:829–835
41. Mao S, Zhang Y, Rohani S, Ray AK (2012) Chromatographic resolution and isotherm determination of (R, S)-mandelic acid on chiralcel-OD column. J Sep Sci 35:2273–2281. https://doi.org/10.1002/jssc.201200322
42. Zhang H, Zhang Z, Hu Y, Yang X, Yao S (2011) Synthesis of a novel composite imprinted material based on multiwalled carbon nanotubes as a selective melamine absorbent. J Agric Food Chem 59:1063–1071
43. Datsyuk V, Kalyva M, Papagelis K, Parthenios J, Tasis D, Siokou A, Kallitsis I, Galiotis C (2008) Chemical oxidation of multiwalled carbon nanotubes. Carbon N Y 46:833–840. https://doi.org/10.1016/j.carbon.2008.02.012
44. Zhang Z, Li Y, Liu X, Zhang Y, Wang D (2018) Molecular imprinting electrochemical sensor for sensitive creatinine determination. Int J Electrochem Sci 13:2986–2995. https://doi.org/10.20964/2018.03.67
45. Tiwari MP, Prasad A (2015) Molecularly imprinted polymer based enantioselective sensing devices : a review. Anal Chim Acta 853:1–18. https://doi.org/10.1016/j.aca.2014.06.011
46. Zhang Q, Guo L, Huang Y, Chen Y, Guo D, Chen C, Fu Y (2014) An electrochemical chiral sensing platform for propranolol enantiomers based on size-controlled gold nanocomposite. Sens Actuators B Chem 199:239–246. https://doi.org/10.1016/j.snb.2014.03.059
47. Chen Z, Tang C, Zeng Y, Liu H, Yin Z, Li L (2014) Determination of bisphenol a using an electrochemical sensor based on a molecularly imprinted polymer-modified multiwalled carbon nanotube paste electrode. Anal Lett 47:996–1014. https://doi.org/10.1080/00032719.2013.862624
48. Rezaei B, Foroughi-dehnavi S, Ensafi AA (2015) Fabrication of electrochemical sensor based on molecularly imprinted polymer and nanoparticles for determination trace amounts of morphine. Ionics (Kiel) 21:2969–2980. https://doi.org/10.1007/s11581-015-1458-3
49. Aravind A, Mathew B (2018) Electrochemical sensor based on nanostructured ion imprinted polymer for the sensing and extraction of Cr (III) ions from industrial wastewater. Polym Int 67:1595–1604. https://doi.org/10.1002/pi.5683
50. Hu Y, Zhang Z, Zhang H, Luo L, Yao S (2012) Selective and sensitive molecularly imprinted sol–gel film-based electrochemical sensor combining mercaptoacetic acid-modified PbS

nanoparticles with Fe3O4@Au–multiwalled carbon nanotubes–chitosan. J Solid State Electrochem 16:857–867. https://doi.org/10.1007/s10008-011-1434-4
51. Karla M, Coelho L, Giarola JDF, Talita A, Ricardo C, Tarley T, Borges KB, Pereira AC (2016) Development and application of electrochemical sensor based on molecularly imprinted polymer and carbon nanotubes for the determination of carvedilol. Chemosensors 4:22–37. https://doi.org/10.3390/chemosensors4040022
52. Alankar S, Vipin G (2011) Methods for the determination of limit of detection and limit of quantitation of the analytical methods. Chronicles Young Sci 2:21–25. https://doi.org/10.4103/2229-5186.79345